

A universal relationship between magnetization and changes in the local structure below T_c in $\text{La}_{1-x}\text{Ca}_x\text{MnO}_3$.

F. Bridges,¹ L. Downward,¹ S. Bushart,¹ J. Neumeier,² N. Dilley,³ and L. Zhou⁴

¹*Physics Department, University of California, Santa Cruz, California 95064, USA*

²*Department of Physics, Montana State University, Bozeman, MT 59717, USA*

³*Quantum Design Inc., 11578 Sorrento Valley Road, San Diego, CA 92121-1311, USA*

⁴*Stanford Synchrotron Radiation Laboratory, Stanford Linear Accelerator Center, Menlo Park, CA 94025, USA*

(Dated: February 13, 2019)

We extend previous X-ray Absorption Fine Structure (XAFS) measurements on $\text{La}_{1-x}\text{Ca}_x\text{MnO}_3$, $x = 0.21, 0.3$, to high B-fields (11T), to investigate a universal relationship between changes in the local structure and the sample magnetization, M. These measurements show that changes in σ^2 for the Mn-O bond near T_c (σ is the width of the Mn-O pair distribution), depend only on M, irrespective of whether the sample magnetization is achieved through a decrease in temperature or an applied B-field. For $x=0.3$, there is still a significant change of σ^2 with T below 150K, (sample fully magnetized); i.e. distortions are clearly present in the magnetized state that are removed as T is lowered further. In the initial development of M, the decrease in σ^2 is small until the sample is roughly 50% magnetized; above 60% the change in σ^2 is much larger. A model for the magnetization process is proposed; it predicts that the magnetization initially develops in a filamentary manner.

PACS numbers: 72.15.Qm, 61.10.Ht, 71.23.-k, 71.27.+a

The quasicubic manganites $\text{La}_{1-x}\text{Ca}_x\text{MnO}_3$ exhibit colossal magnetoresistance (CMR) for Ca concentrations $\sim 20\text{-}50\%$. Within this concentration range there are significant local structural changes as a function of temperature near the ferromagnetic transition temperature T_c , observed both macroscopically (changes in the lattice constants) and at the local atomic level (changes in the Mn-O pair distribution function (PDF)). These local distortions are associated with polarons and decrease rapidly through and below the ferromagnetic transition as observed using XAFS[1, 2, 3, 4, 5, 6, 7, 8] and neutron PDF analysis[9, 10, 11] at $B=0\text{T}$. Many authors have argued for a phase separation[12, 13, 14, 15, 16, 17] (or two fluid[3, 18]) model, formed of conducting, ferromagnetic clusters/regions and poorly conducting regions. However, the microscopic details of the initial nanoscale clusters and how they develop into a fully magnetized state is still poorly understood.

Previously we have shown that the decrease in σ^2 , $\Delta(\sigma^2)$, as T is decreased below T_c is a simple function of the sample magnetization, M[3] - however those measurements were at low or zero magnetic field and T was a hidden parameter - i.e. each point in the plot of $\Delta(\sigma^2)$ vs M was at a different value of T. We and others have shown that at low B-fields ($\sim 1\text{T}$), there is a small B-field induced local structure change near T_c [7, 19]. Here we extend those measurements to high fields, 9-11T, and show that a universal relationship exists between $\Delta(\sigma^2)/(\Delta(\sigma^2))_0$ and M/M_0 [$(\Delta(\sigma^2))_0$ is the overall change down to the temperature at which $M/M_0 \sim 1$; M_0 is the saturation magnetization]. Some preliminary results for the 21% sample were presented earlier[20]. In addition to the universality for a given sample, we show three important results: 1) in the initial develop-

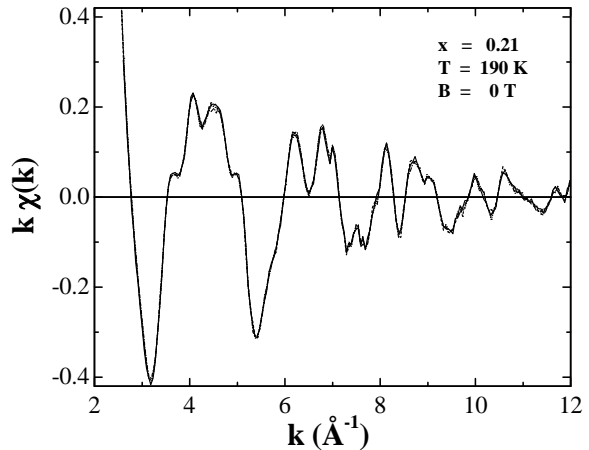


FIG. 1: k-space plots. Four scans are overlaid to show the reproducibility of the data

ment of the magnetization ($M/M_0 < \sim 0.5$), relatively little distortion is removed, 2) the breakpoint at which $\Delta(\sigma^2)/(\Delta(\sigma^2))_0$ increases more rapidly with M/M_0 , increases with Ca concentration x, (it occurs when $M/M_0 \sim 2x$), and 3) that in at least one sample, some local distortion (larger than the expected thermal phonon contribution) is present even when the sample is fully magnetized. This aspect has been controversial but is very clearly shown in the high field data. The first two results lead to a proposed model in which the magnetization develops as filamentary clusters in the sample.

XAFS Mn K-edge data were collected on powdered samples at the Stanford Synchrotron Radiation Laboratory (SSRL), using Si(111) double monochromator crystals on beam line 7-2. The data were collected in transmission mode as a function of temperature and applied magnetic

field (up to 11T). For the XAFS samples, the pressed material was reground, passed through a 400-mesh sieve, and then brushed onto scotch tape which preferentially holds the smaller grains ($\leq 5 \mu\text{m}$). Layers of tape were stacked to obtain absorption lengths such that the step height $\mu_{\text{Mn}} t \sim 0.5$ for each sample. Generally, four scans were collected at each T and B-field for each sample.

The absorption from other atoms (pre-edge absorption) was removed by fitting the data above and below the edge to a Victoreen formula; then a sum of splines was used to obtain the background μ_0 above the edge[21, 22]. The XAFS oscillations, χ were then obtained as a function of photoelectron wave vector $k = \sqrt{2m_e(E - E_0)/\hbar^2}$ from $\chi(k) = \mu/\mu_0 - 1$. In Fig. 1 we overlay 4 k-space traces of $k\chi(k)$ to show the reproducibility of the data; data for $k > 12 \text{ \AA}^{-1}$ were precluded because of a small amount of Fe (Fe K-edge at 7112eV) in the Be can of the high field cryostat. The $k\chi(k)$ data were then Fourier transformed (FT) to r-space.

In Fig. 2 we plot the Fourier transformed data (first Mn-O peak only) for the 21% and 30% Ca samples at several fields near T_c . As the field increases, the amplitude of the Mn-O peak increases; thus the average value of σ must decrease. In contrast, for low T or $T \gg T_c$, no significant B-field induced change in σ is observed.

The r-space data were fit[22] to similarly transformed standard functions, calculated using the FEFF6 code[23]. In these fits we used the values of E_0 and S_0^2 determined in earlier studies, constrained the number of neighbors to 6, and fit the first Mn-O peak using an average bond length and a single broadening parameter, σ . The latter provides a single-parameter-measure of the local structural disorder for comparisons with M. Although one can model the system as two Mn-O peaks[8], that would require two amplitudes and two σ 's which are partially coupled; then a local structure parameter for comparison with M is not well defined. For each temperature, separate fits were made to four traces and the average value of σ calculated; the rms fluctuation about the average, gives the relative errors, which are comparable to the symbol size in most cases (See Fig. 3). The absolute errors for σ^2 , depend on the error in S_0^2 which may be of order 10-15 %; this error primarily changes the static component to σ^2 , and shifts the σ^2 vs T plot vertically.

$\sigma^2(T)$ for the Mn-O peak is plotted in Fig. 3 for each sample at various fields. For the 21% sample the curves shift to higher T and broaden as B increases, and the B-field induced changes extend down to 50K. For the 30% sample the behavior is similar above T_c - a broadening and shift of the curve to higher T - but the effect appears non-uniform, mainly because of the much sharper magnetic transition for this sample. Below T_c the magnetization rapidly approaches M_0 and is essentially constant below 150K (Fig3, lower inset). However there is still a decrease observed for $\sigma^2(T)$ that is much faster than ex-

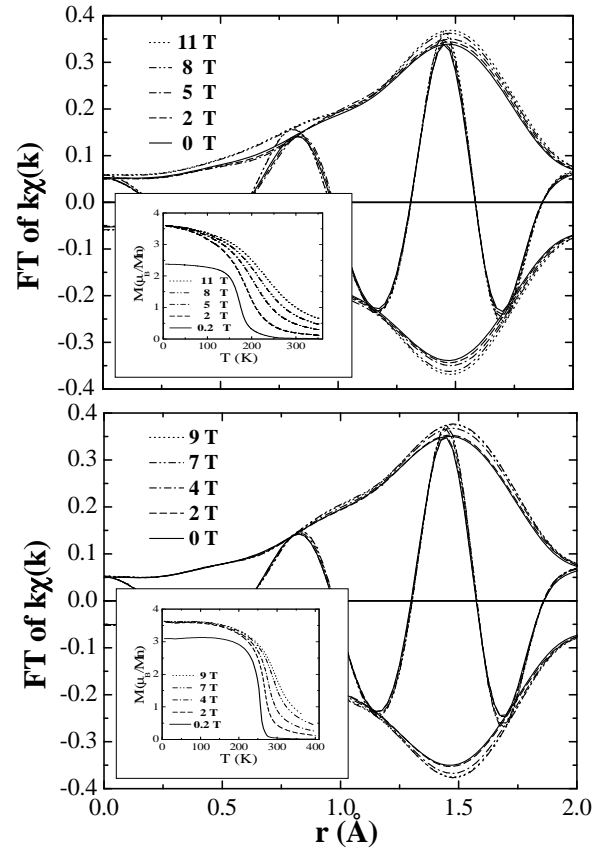


FIG. 2: The r-space peak for the Mn-O bond (21% Ca (top) and 30% Ca sample (bottom)) at different fields near T_c (21% - $T_c \sim 190\text{K}$; 30% - $T_c \sim 270\text{K}$). The fast oscillation is the real part of the transform (FT_R) while the envelop is $\pm\sqrt{FT_R^2 + FT_I^2}$ where FT_I is the imaginary part of the FT. The FT range is 3.5-11.5 \AA , with 0.3 \AA^{-1} Gaussian broadening. The inset shows the corresponding changes in the magnetization for each sample. As the applied field is increased, the “transition” becomes broader and moves to a higher temperature.

pected from thermal phonons. We emphasize that XAFS is a very fast probe (10^{-15} sec scale) as a result of the short core-hole lifetime; consequently even the fastest lattice distortions are observed in contrast to slower probes such as neutron diffraction. The important result here is that the hopping rate is sufficient for the double exchange interaction (or other magnetic coupling) to be effective, yet it appears that the hopping of the polarons is still slow enough that the lattice can have a small response. As the sample cools further, scattering decreases, the electrons hop faster and the remaining distortion decreases. Thus because XAFS is such a fast probe we may be observing the last remnants of the polaron distortion below 100K. The same process probably also occurs for the 21% sample (and may account for the larger scatter in the plot of $\Delta(\sigma^2)$ - Fig. 4: top) but is masked because full magnetization is not achieved till $\sim 20\text{K}$ - perhaps from a distribution of T_c s, or possibly the pres-

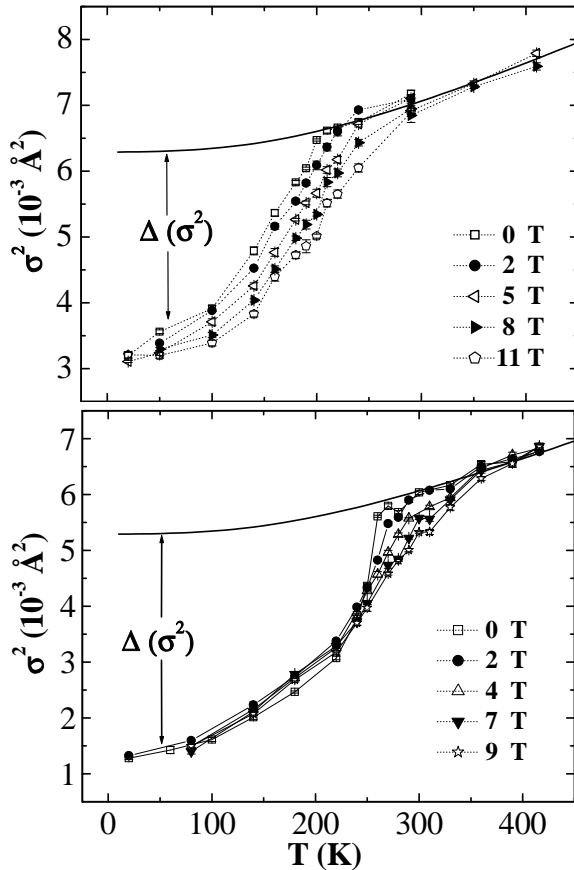


FIG. 3: σ^2 vs T for the first Mn-O peak at several magnetic fields; 21% Ca (top) and 30% Ca (bottom). The dotted lines are guides to the eye. The solid line is the behavior if no polaron distortions are removed - i.e. σ^2 for CaMnO_3 plus a large static distortion.

ence (above 20K) of small, antiferromagnetically-coupled clusters where the local Ca doping is low. Additional experiments on higher doping level samples are needed to probe this further.

Using $\sigma^2(T)$ from Fig 3 and $M(T)$ (insets in Fig. 2) we can investigate the relationship between changes in the local distortions and the sample magnetization. The contributions to $\sigma^2(T)$ add up in quadrature when different broadening mechanisms are uncorrelated, i.e;

$$\sigma^2(T) = \sigma_{\text{phonons}}^2(T) + \sigma_{\text{static}}^2 + \sigma_{\text{polaron}}^2(T) \quad (1)$$

where $\sigma_{\text{phonons}}^2(T)$ is the contribution from thermal phonons, σ_{static}^2 arises from static distortions, and $\sigma_{\text{polaron}}^2(T)$ is the contribution from the presence of hopping polarons. The latter become T-independent when $M \sim 0$ - we refer to this as $\sigma_{\text{full-polaron}}^2$; the remaining T dependence at high T is nearly identical to that for pure CaMnO_3 [3] and arises from the phonon contribution. For a comparison purposes, we need the decrease in $\sigma^2(T)$, $\Delta(\sigma^2)$, as the magnetization increases; this is defined as the difference between the solid line in Fig. 3 and the data. In Fig. 4 we plot $\Delta(\sigma^2)/(\Delta(\sigma^2))_0$ vs M/M_0 ; most

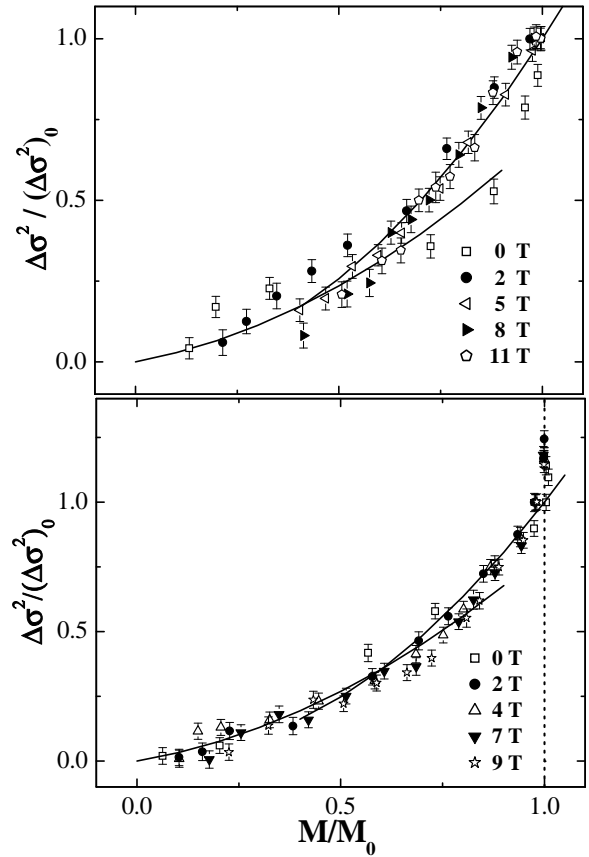


FIG. 4: $\Delta(\sigma^2)$ vs relative magnetization for the 21% Ca (top) and the 30% Ca sample (bottom) at different magnetic fields. $\Delta(\sigma^2)$ and M have been normalized to their respective values when $M/M_0 \sim 1$ at low temperature, see Fig. 3 and magnetization curves in the inset of Fig. 2. $\Delta(\sigma^2)$ is the decrease in σ^2 as T is lowered below T_c that is attributed to the loss of polaronic distortion. The solid lines represent the model discussed in which the sample initially becomes magnetized in pairs, i.e. $\Delta(\sigma^2)$ is a quadratic function of magnetization.

of the data fall on the same line within the errors, irrespective of whether the magnetization was obtained by a change in B or T. Thus the distortions removed are a universal function of the sample magnetization. An important feature of this linear plot is that little distortion is removed until the sample is 40-60% magnetized; the largest local distortion changes occurs for $M/M_0 > 0.6$. The break point occurs when M/M_0 is slightly larger than 2x (twice the number of holes) which suggests that the sample initially becomes magnetized in Mn pairs (an undistorted hole site and a distorted electron site).

For the double exchange mechanism to be operative a charge carrier must be able to rapidly hop back and forth between two sites. This can't happen for two electron (or hole) sites but can for a hole/electron pair. For the Jahn-Teller (JT) distorted site it costs energy E_{JT} , to undistort the site; consequently as long as holes are present, the least amount of energy is required when the magnetization develops in hole/electron site-pairs. If we

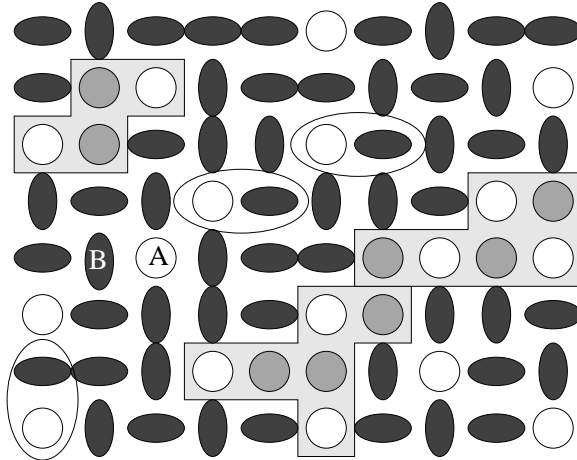


FIG. 5: Model of magnetization process. Open circles- holes; black ovals - JT distorted polarons; outlined regions - magnetic clusters; gray circles - magnetized electron sites, for which J-T distortion removed.

let the distortion per JT-site be α , then the distortion removed per magnetized Mn site is only $\alpha/2$ in the initial stages of magnetization, but once the holes are used up, the distortion removed per Mn site then increases to α . This is very close to the behavior of the data shown in Fig. 4; however the ratio of the slopes at high and low M is slightly larger than 2 in the data. We propose that this is the result of different distortions and different values of E_{JT} throughout the system as a result of strains and local variations in Ca content. The sites with the lowest values of E_{JT} (smallest distortions) would become magnetized first. To model this aspect we let the distortion per Mn site that is removed depend on the fraction f of magnetized sites; $f = M/M_0$. Then for a simple linear dependence, $\alpha = \alpha_0(1 + \gamma f)$ with γ a constant, and

$$\frac{\Delta(\sigma^2(f))}{(\Delta(\sigma^2))_0} = \begin{cases} \frac{\frac{1}{2}\alpha f}{N} & f \leq 2x \\ \frac{\frac{1}{2}\alpha(2x) + \alpha(f-2x)}{N} & f > 2x \end{cases} \quad (2)$$

where the normalization factor N which depends on α_0 , is chosen to make $\Delta(\sigma^2(f))/(\Delta(\sigma^2))_0 = 1$ at $f = 1$. A value of $\gamma = 2$ (α varies from α_0 to $3\alpha_0$) generates the curves in Fig. 4.

A “cartoon” of this model for $T \sim T_c$ is depicted in Fig. 5. Possible pairs of undistorted holes (open circles) and JT distorted electron Mn sites (black ovals) are encircled with ovals at some instant in time. However the holes are continuously hopping and the (unmagnetized) pairs are continually changing. Several magnetized clusters are also shown: in each cluster the electron sites next to the holes become undistorted (represented by gray circles). At this point the electrons in the magnetic cluster will of course become delocalized but we keep pairs of (undistorted) open and gray circles for counting purposes. For low M ($M/M_0 < 0.4$) the holes in the non-magnetic matrix are continually hopping and will occasionally diffuse

close enough to a magnetic cluster that another pair can join the cluster; for example if hole A hops to position B, another pair of Mn atoms could connect to the upper magnetic cluster and become magnetic. Thus the cluster development in this regime may be similar to diffusion limited aggregation, with the majority of the magnetic thermal fluctuations occurring in the paramagnetic and boundary regions. It will lead to interpenetrating (magnetic and non-magnetic) filamentary clusters.

In summary we have presented XAFS data as a function of B and T which indicate that the decrease in lattice distortion with sample magnetization is a universal function. The initial decrease in distortion is small up to $M/M_0 \sim 2x$ which suggests that the magnet clusters develops by adding Mn pairs (a hole site and a J-T site). This leads to filamentary clusters for $M/M_0 < 0.5$. Also for the 30% sample, distortions are still present at low T , in the fully magnetized sample - the very fast XAFS probe allows one to see these last vestiges of the polaron distortions. Note, the double exchange mechanism is still operative even with distortions present. Additional measurements for a range of Ca concentrations from 0.3-0.49, are needed to determine how the break point in Fig. 4 moves with Ca concentration and to explore the remaining polaron distortions at low T . We anticipate that these results will stimulate further theoretical calculations.

The work at UCSC was supported in part by NSF grant DMR0301971. The experiments were performed at SSRL, which is operated by the DOE, Division of Chemical Sciences, and by the NIH, Biomedical Resource Technology Program, Division of Research Resources.

- [1] C. H. Booth *et al.*, Phys. Rev. B **54**, R15606 (1996).
- [2] C. H. Booth *et al.*, Phys. Rev. Lett. **80**, 853 (1998).
- [3] C. H. Booth *et al.*, Phys. Rev. B **57**, 10440 (1998).
- [4] G. Subías *et al.*, Phys. Rev. B **56**, 8183 (1997).
- [5] T. A. Tyson *et al.*, Phys. Rev. B **53**, 13985 (1996).
- [6] D. Cao *et al.*, Phys. Rev. B **61**, 11373 (2000).
- [7] D. Cao *et al.*, Phys. Rev. B **62**, 8954 (2000).
- [8] A. Lanzara *et al.*, Phys. Rev. Lett. **81**, 878 (1998).
- [9] S. J. L. Billinge *et al.*, Phys. Rev. Lett. **77**, 715 (1996).
- [10] D. Louca *et al.*, Phys. Rev. B **56**, R8475 (1997).
- [11] D. Louca *et al.*, J. Superconductivity **12**, 291 (1999).
- [12] E. Dagotto *et al.*, Phys. Rev. B **58**, 6414 (1998).
- [13] A. Moreo *et al.*, Science **283**, 2034 (1999).
- [14] J. Burgoy *et al.*, Phys. Rev. Lett. **92**, 097202/1 (1992).
- [15] A. R. Bishop, *et al.*, Europhys. Lett. **63**, 289 (2003).
- [16] A. Weisse, J. Loos, and H. Fehske, Phys. Rev. B **68**, 024402/1 (2003).
- [17] Y. Motome *et al.*, Phys. Rev. Lett. **91**, 167204/1 (2003).
- [18] S. K. Sarker, J. Phys.: Condens. Matter **8**, L515 (1996).
- [19] C. Meneghini *et al.*, J. Phys.: Condens. Matter **14**, 1967 (2002).
- [20] L. Downward *et al.*, Inter. J. Mod. Phys. **17**, 3726 (2003).
- [21] G. G. Li, *et al.*, Phys. Rev. B **52**, 6332 (1995).
- [22] Website: (<http://lise.lbl.gov>) for r-space EXAFS data analysis package.
- [23] S. I. Zabinsky *et al.*, Phys. Rev. B **52**, 2995 (1995).